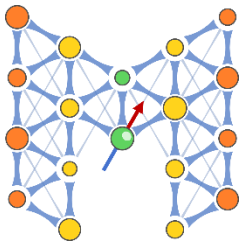

MANNGA Deliverable

D2.3 Report on phenomenological modelling of devices in T2.1 and T2.2, accompanied by a code for the model's implementation, a summary of its validation against micromagnetic results, a summary of examples of its application to physical devices, and an updated rank-list from MS2.3b.

Version 1.0

Grant Agreement number	101070347
Action Acronym	MANNGA
Action Title	MAGNONIC ARTIFICIAL NEURAL NETWORKS AND GATE ARRAYS
Call	HORIZON-CL4-2021-DIGITAL-EMERGING-01
Version date of the Annex I against which the assessment will be made	31.5.2022
Start date of the project	1.9.2022
Due date of the deliverable	30.11.2023
Actual date of submission	22.12.2023
Lead BEN / AP for the deliverable	UNEXE
Dissemination level of the deliverable	Public

Coordinator, PI
Sebastiaan van Dijken
AALTO KORKEAKOULUSÄÄTIÖ SR, Aalto University School of Science

Scientific coordinator
Volodymyr Kruglyak
THE UNIVERSITY OF EXETER

Co-funded by the European Union

MANNGA project is partly funded by the European Union. Views and opinions expressed are however those of the author(s) only and do not necessarily reflect those of the European Union or HADEA. Neither the European Union nor the granting authority can be held responsible for them.

Authors in alphabetical order		
Name	Beneficiary	e-mail
Kevin Fripp	The University of Exeter (UNEXE)	K.G.Fripp@exeter.ac.uk
Volodymyr Kruglyak	The University of Exeter (UNEXE)	V.V.Kruglyak@exeter.ac.uk
Andrey Shytov	The University of Exeter (UNEXE)	A.Shytov@exeter.ac.uk

Document reviewers		
Name	Beneficiary	e-mail
Sebastiaan van Dijken	Aalto University	sebastiaan.van.dijken@aalto.fi

Executive summary
This deliverable reports on MANNGA's development and validation of a powerful phenomenological model by which to describe and to predict properties of different types of magnonic resonators to be used in the project. The current version of the model is valid for isolated resonators, while its generalisation to multiple resonators will be developed in work package WP3 and is already under way.

Contents

1. Introduction: The aims and objects of the phenomenological modelling in T2.3

MANNGA's Task T2.3 aims to create phenomenological models capable of quantitative description of devices from Tasks T2.1 (transition metal chiral magnonic resonators, CMRs, on continuous YIG media) and T2.2 (all-YIG CMRs) in terms of spin-wave (SW) scattering from CMRs, including non-linear effects. From has already been known from the start that the use of different magnetic materials for CMRs in T2.1 and T2.2 should lead to distinctly different regimes of the CMR performance. Within T2.1, the high frequencies of the Kittel and higher-order SW modes of the transition-metal based CMRs prevent them from interacting resonantly with SWs propagating in YIG, and so, magnonic Fabry-Perot resonances are formed instead in the YIG medium underneath the CMRs. In T2.2, the use of YIG for both the CMR and the medium enables frequency matching and resonant interaction between their localised and propagating SW modes, respectively. The phenomenological model developed in Task T2.3 and outlined below can describe both types of the CMR behaviour on the same footing and predict design outcomes in terms of relative merits and weakness of using each of the approaches in different scenarios.

2. Brief description of the approach

The system's dynamics is sub-divided into SW modes of the medium and local oscillators representing individual SW modes localised in the CMR. Each mode is formalised separately, with the local oscillators exhibiting nonlinearity and the propagating modes of the medium always remaining linear. The magneto-dipolar coupling between the different modes may then lead to scattering of the propagating modes and resonant energy concentration in the localised modes. This energy concentration may lead to a nonlinear shift of the localised mode's frequency and associated nonlinear variation of the scattered intensity of the propagating modes. Our phenomenological model accounts for the localised mode's profile, the mode's frequency shift and line broadening due to coupling to propagating modes in the medium, as well as resonant and non-resonant coupling between multiple SW modes of the resonator and medium, including those characterised by anti-Larmor precession. The developed phenomenological mode is implemented within a Python code, which is available from https://github.com/avshytov/MANNGA-Spin-Wave-Scattering. Expectedly, the code runs drastically faster and has a reduced memory footprint as compared to full micromagnetic simulations. When assembling individual CMRs into arrays at later stages of MANNGA, additional speed-up can be achieved by "switching off" parts of the code that do not produce a significant effect for a particular device design. In meantime, this feature of the code has already been useful in elucidating physics leading to different effects observed in our devices and explaining connections between different aspects of the extremely complex dynamics.

3. Examples of validation of the model

To validate the model, its predictions are compared to results of micromagnetic simulations performed using MuMax3 software. The validity of the simulations themselves is checked by modelling experimental data described e.g. in D2.1, with a good agreement observed.

3.1 CoFeB-based Fabry-Perot resonators (Task T2.1)

We begin by comparing the model's results with those obtained for a CoFeB Fabry-Perot resonator system for which a good agreement between the experiment and micromagnetic simulations has already been established. The comparison is presented in Fig. 1. The agreement is excellent. Moreover, the phenomenological model predicts that the feature at around 0.7-0.8 GHz frequency is a real resonance, which has been overlooked previously (due to the noise) both in the simulations and experiments. The measurements are now being extended to the lower frequencies.

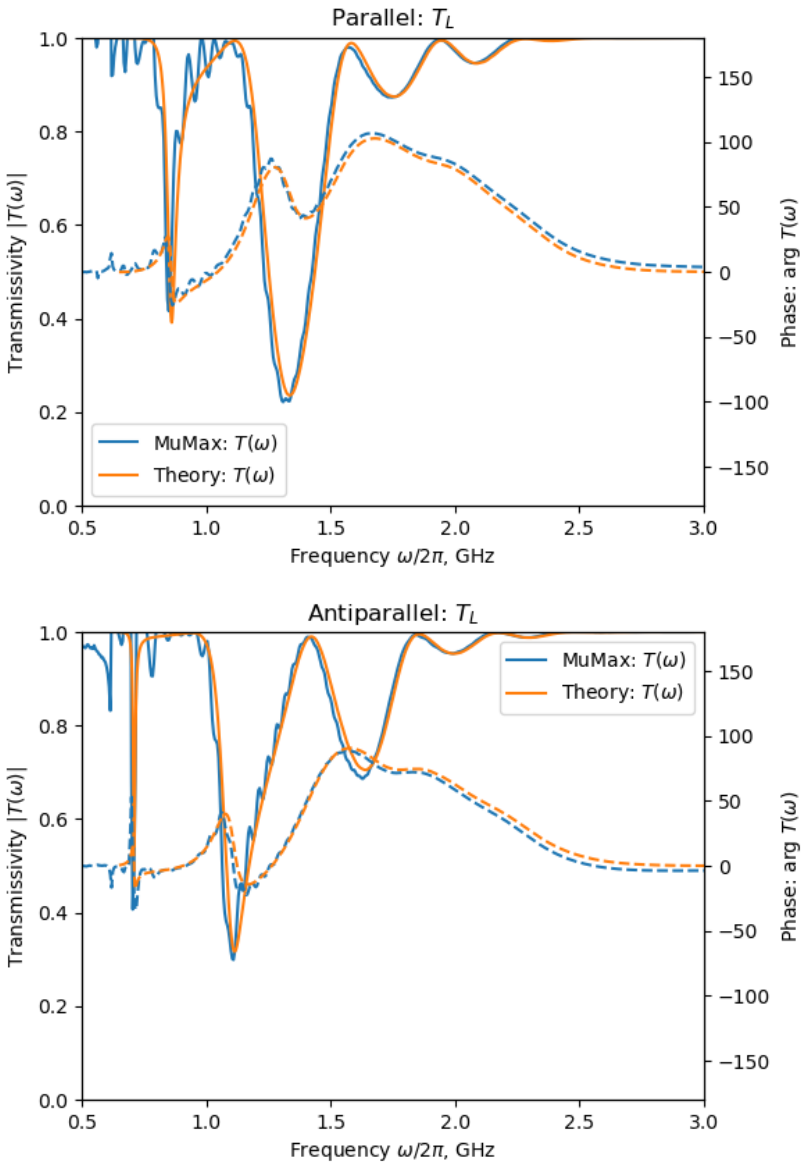

Figure 1. The amplitude and phase of the simulated (blue) and analytical (red) transmission coefficients are shown for different directions of the SW incidence on a CoFeB/YIG Fabry-Perot resonator system with a parallel (top) and antiparallel (bottom) alignment of the magnetizations in the resonator and the medium.

3.2 All-YIG chiral magnonic resonators (Task T2.2)

To validate the model's performance for all-YIG structures, representative results of the phenomenological model and MuMax simulations for an all-YIG structure are plotted in Fig. 2. The reassuring agreement between the simulated and analytical results enables to use our analytical model to explore the parameters space in order to design all-YIG structures that would produce optimal behaviour in experiments – see Section 4.3 below.

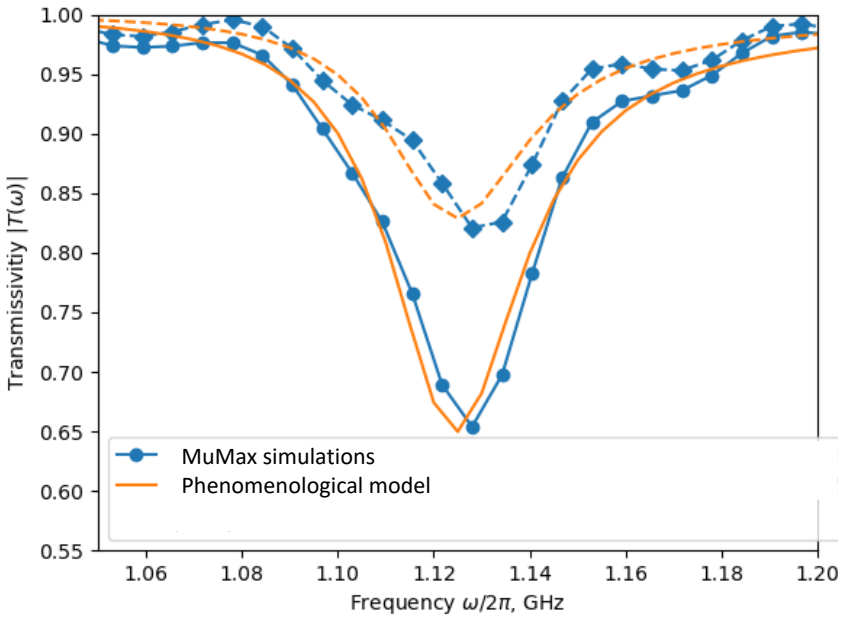

Figure 2. The SW transmissivities predicted by MuMax simulations (blue lines with symbols) and by phenomenological modeling (red lines) are shown for different directions of the SW incidence on an all-YIG resonator system with an antiparallel alignment of the magnetizations in the resonator and the medium.

3.3 Nonlinear all-Permalloy chiral magnonic resonators as magnonic neurons

The third stage of validation of the model concerned its ability to describe non-linear SW scattering. Figure 3 presents the results of using the model to fit SW transmission coefficient obtained from micromagnetic simulations of 1D all-Permalloy chiral magnonic resonators. Excellent agreement is evident for all values of the incident SW amplitude. The full account of this study is published in Ref. 1. The physics underpinning the nonlinear modification of the SW scattering coefficients is expected to remain the same in the different types of CMRs explored in MANNGA and arrays of those, and so, the model will remain applicable.

[1] K. G. Fripp, et al, "Nonlinear chiral magnonic resonators: Toward magnonic neurons" Appl. Phys. Lett. **122**, 172403 (2023); doi: 10.1063/5.0149466.

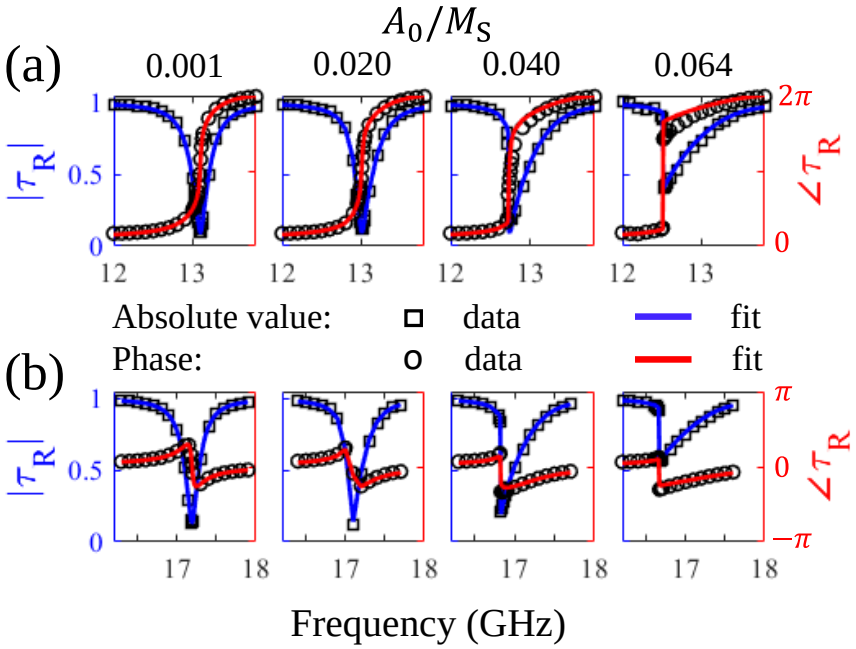

Figure 3. The amplitude and phase of the simulated transmission (symbols) and corresponding fits to the phenomenological model (lines) are shown for different SW amplitudes and frequencies near the resonator's (a) quasi-uniform and (b) dark mode.

4. Other examples of the model's application

Further validation and development of the phenomenological model will continue through its application to systems for which no comprehensive experimental or numerical data is available. In such cases, the phenomenological modelling is used to generate predictions and designs, which will be tested experimentally and / or numerically in the rest of the project.

4.1 Two-dimensional scattering of spin waves by Permalloy-based chiral magnonic resonators

Although the example of the model's validation above were all for 1D systems, the model is also capable of describing 2D scattering of spin waves. So, Figure 4 shows a directivity diagram obtained for resonant SW scattering from a 60 nm Permalloy element located 40 nm above a 50 nm thick YIG film. The agreement between the phenomenological theory and numerical simulations is more modest in this case. The discrepancy is currently attributed to the limitations of the numerical simulations, which are in turn limited by the hardware used to run them. In addition, both approaches revealed a significant sensitivity of the obtained results to the edge quality of the nanoscale elements. This suggests that the most reasonable strategy to the problem would be based on the experiment, with the theory applied to describe measured results and thereby either to validate the methodology used or to spur its refinement and further development.

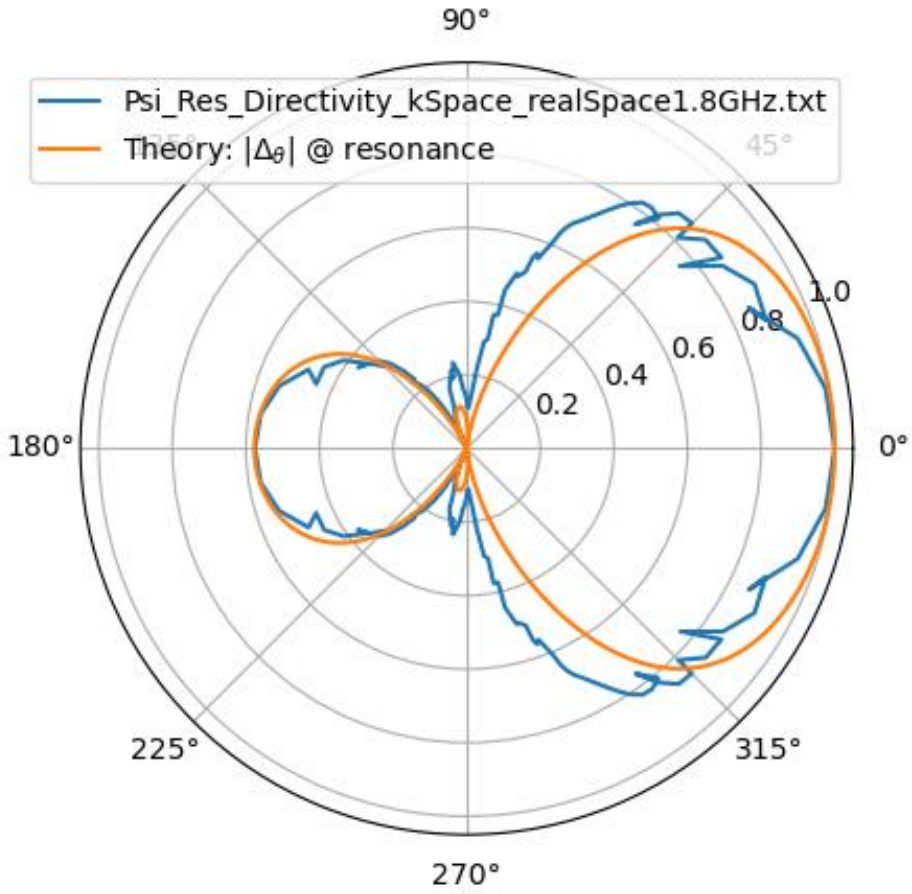

Figure 4. The reciprocal-space directivity diagrams obtained using micromagnetic simulations (blue) and phenomenological modelling (orange) are shown for resonant SW scattering from a 60 nm Permalloy element located 40 nm above a 50 nm thick YIG film.

4.2 Establishing relationship between Fabry-Perot and localised mode-based chiral magnonic resonators.

The reassuring agreement between the phenomenological modelling, numerical simulations, and experiments observed for magnonic Fabry-Perot resonators enables us to use the model for mapping the parameter space, identifying optimal device designs, and revealing new physics. An example of this is shown in Fig. 5, where the effects of the magnetisation's length and orientation in the stripe located above a YIG film are explored. The range of the magnetisation variation in Fig. 5 covers both the CoFeB and YIG values, although the exchange constant is fixed at the CoFeB value. The pseudo-colour maps of the SW transmissivity reveal not only dips associated with low-frequency narrow and higher-frequency broad Fabry-Perot resonances but also those due to resonant coupling of propagating SWs with localised SW modes of the stripe at higher frequencies and lower magnetisation values. The latter features show an enhanced chirality as compared to those caused by Fabry-Perot resonances. The narrow resonances of both types can be used to concentrate the energy of the incident SWs and therefore to design artificial magnonic neurons.

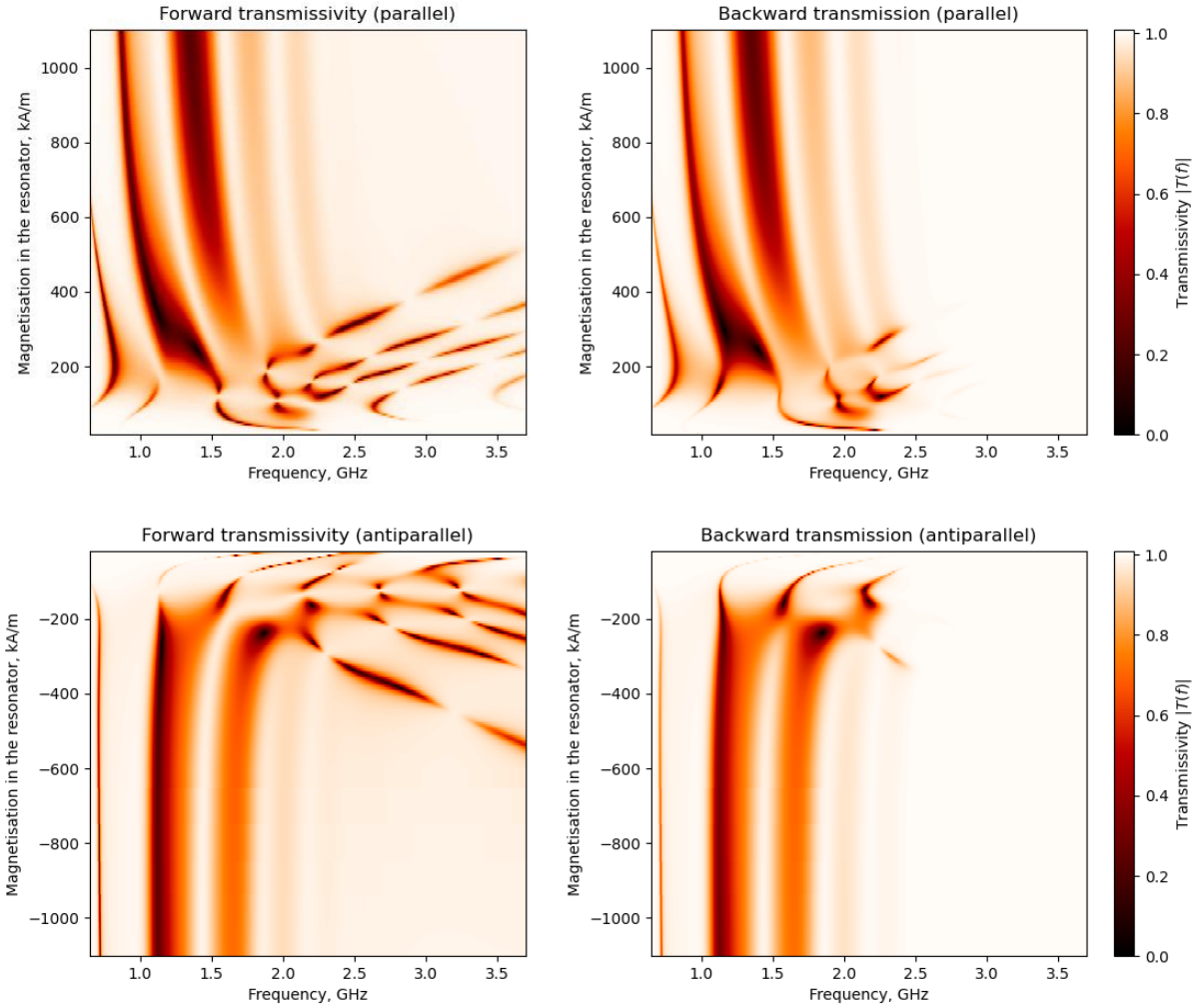

Figure 5. Pseudo-colour maps of the SW transmissivity are shown as a function of the incident SW frequency and the magnetisation of the ferromagnetic stripe forming the Fabry-Perot resonator. The different panels correspond to the different combinations of the mutual orientations of the magnetisation in the stripe and the directions of the SW incidence. The negative values of the magnetisation signify the negative direction of the stripe's magnetisation relative to that in YIG.

5. Final remarks

In summary, we have developed and validated a powerful phenomenological model by which to describe and to predict properties of different types of magnonic resonators to be used in MANNGA. The current version of the model is valid for isolated resonators, while its generalisation to multiple resonators will be developed in work package WP3 and is under way. Once milestone CMS2.3b "CMS2.3b: The CMR models are applied to available data from fabricated and tested CMR devices, which are compared and rank-ordered (by achieved and expected KPIs, and time and effort of their fabrication) for use in WP3" has been achieved, this deliverable will also be updated accordingly.